JOURNAL OF PHYSICAL ORGANIC CHEMISTRY
J. Phys. Org. Chem. 2002; **15:** 123–129
DOI:10.1002/poc.460

Rate constants for the $CH_3O + NO \rightarrow CH_3ONO$ reaction by classical trajectory and canonical variational transition state theory calculations

Emilio Martínez-Núñez,[1]* Itamar Borges Jr[2] and S. A. Vázquez[1]

[1]Departamento de Química Física, Universidad de Santiago de Compostela, Santiago de Compostela E-15706, Spain
[2]Instituto de Química, Departamento de Físico-Química, Universidade Federal de Rio de Janeiro, 21949-900, Rio de Janeiro-RJ, Brasil

Received 22 May 2001; revised 5 August 2001; accepted 7 September 2001

ABSTRACT: Classical trajectory and canonical variational transition state theory (CVTST) calculations were performed on the $CH_3O + NO \rightarrow CH_3ONO$ recombination reaction for the temperature range 300–1000 K to study theoretically this reaction for the first time. The dynamics calculations employ our previously reported potential energy surface for the dissociation and elimination reactions of methyl nitrite (Martínez-Núñez E, Vázquez SA. *J. Chem. Phys*. 1998; **109**: 8907). In the present work this surface was conveniently modified to reproduce more accurately the experimental CH_3O—NO dissociation energy and to obtain more reliable rate constants for both the dissociation and the recombination reactions. The recombination rate constants calculated with this modified version of the original potential energy surface agree better with the experimental results than do the rates obtained with the original one. Copyright © 2001 John Wiley & Sons, Ltd.

KEYWORDS: methyl nitrite; recombination reaction; thermal rate constants; classical trajectory calculations; CVTST calculations; potential energy surface

INTRODUCTION

There have been many experimental studies of the methoxy (CH_3O) + nitric oxide (NO) reaction.[1–13] This reaction is a prototype radical–radical reaction that can give rise to two different reaction channels: first, the recombination reaction to form chemically activated methyl nitrite (CH_3ONO^*)

$$CH_3O + NO \rightarrow CH_3ONO^* \qquad (1)$$

which is the subject of the present study, and, second, the direct disprotonation channel:

$$CH_3O + NO \rightarrow CH_2O + HNO \qquad (2)$$

The CH_2O and HNO products can also be obtained *via* the chemically activated methyl nitrite molecule as follows

$$CH_3O + NO \underset{b}{\overset{a}{\rightleftarrows}} CH_3ONO^* \xrightarrow{c} CH_2O + HNO \qquad (3)$$

Experimental studies have been devoted to measuring the rate constants for the above reactions in a moderately wide range of temperatures and pressures. Frost and Smith[8] determined the rate constant for the reaction $CH_3O + NO$ in the pressure range 3–100 Torr of argon and for temperatures ranging from 296 to 573 K by using laser-induced fluorescence. They arrived at the following high-pressure limit expression: $k_\infty = 3.6 \times 10^{-11}(T/298)^{-0.6}$ cm^3 molecule^{-1} s^{-1}. They also concluded that the formation of CH_2O and HNO can only occur *via* rearrangement of energized methyl nitrite [(3)]. By contrast, McCaulley *et al.*[9] used a discharged flow reactor to measure the methyl nitrite yield of the $CH_3O + NO$ reaction at 297 K and low pressures (0.5 and 1 Torr) and concluded that under these experimental conditions the direct disprotonation channel, Eqn. (2), is the major one. More recently, Ohmori *et al.*[10] determined the values of the rate constant at room temperature through laser-induced fluorescence, and employing Lindemann–Hinshelwood theory extrapolated their results to the high-pressure limit to obtain $k_\infty = (4.5 \pm 1.5) \times 10^{-11}$ cm^3 molecule^{-1} s^{-1} at 296 ± 6 K. In the most recent work, Caralp *et al.*[13] used discharge flow (DF) and pulsed laser photolysis (PLP) techniques and by means of RRKM calculations, based on their own *ab initio* data, derived the following expression for the limiting high-pressure rate constant: $k_\infty = (3.4 \pm 0.4) \times 10^{-11}(T/298)^{-0.75}$ cm^3 molecule^{-1} s^{-1} in the temperature range 220–600 K.

**Correspondence to:* E. Martínez-Núñez, Departamento de Química Física, Facultade de Ciencias Lagoas-Marcosende, 36200 Vigo, Spain. E-mail: qfemilio@uvigo.es
Contract/grant sponsor: Ministerio de Ciencia y Tecnología, Spain; *Contract/grant number:* BQU 2000-0462.

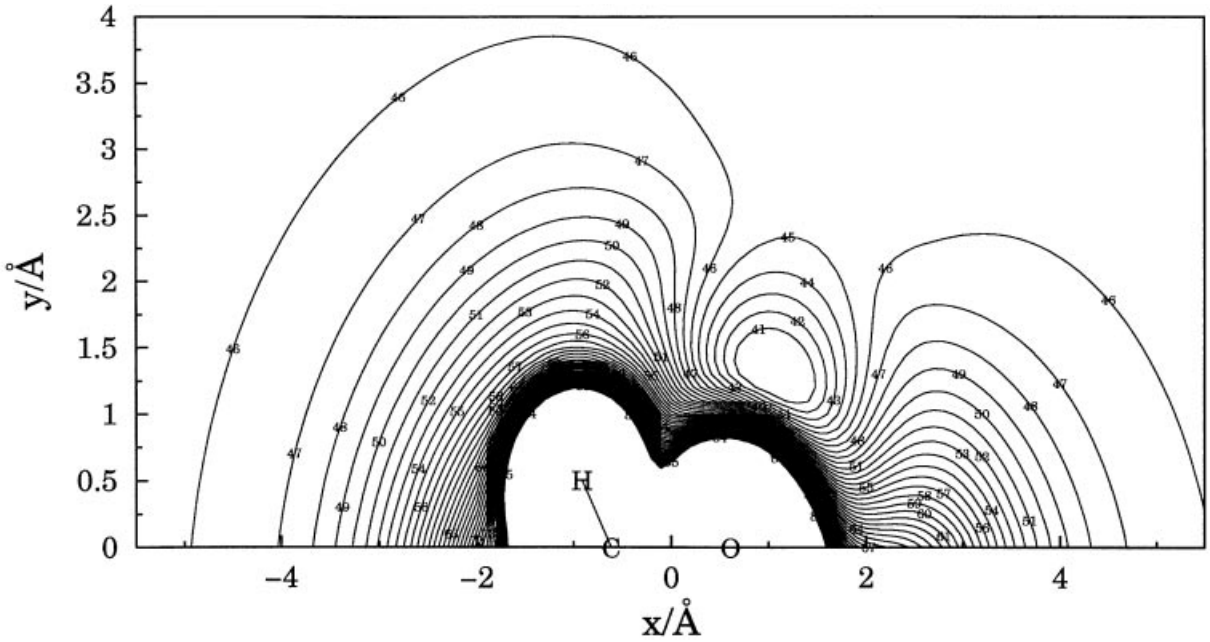

Figure 1. Contour plot for relaxed nitric oxide (NO) moving around the equilibrium methoxy (CH_3O) molecule. Contours start at 20 kcal mol^{-1} with successive contours at intervals of 5 kcal mol^{-1} (being the zero of energy for the CH_3ONO equilibrium geometry)

In the atmosphere, the main sink of the methoxy radical (CH_3O) is its reaction with O_2, whereas at combustion temperatures CH_3O can also decompose unimolecularly ($CH_3O \rightarrow CH_2O + H$) or react with H, O or OH. However, in laboratory studies (smog chambers or shock tubes) the decomposition of methyl nitrite CH_3ONO is a very common source of methoxy and relative measurements involving this radical often use the title reaction as a reference. In fact, several elementary steps in the kinetic modeling of methyl nitrite pyrolysis[7] involve this radical.

Recently, two of us studied the elementary steps **b** and **c** of Eqn. (3) by both classical trajectory calculations[14] and transition state theory.[15] The calculations of the former study concern microcanonical rate constants, whereas the latter involves canonical rate constants. In the present study we shall concentrate on the calculation of the $CH_3O + NO \rightarrow CH_3ONO^*$ recombination rate constant and its temperature dependence. We use our previously reported potential energy surface (PES)[14] and a modified form of it for the present work along with classical trajectories and canonical variational transition state theory (CVTST) to compute thermal rate constants in the 300–1000 K temperature range. This work complements the experimental results, which are not available for the whole range of temperatures studied here.

PES

Our reported PES for methyl nitrite,[14] which accounts for the $CH_3O + NO$ and $CH_2O + HNO$ dissociation channels, was used in the present study. This analytical PES is expanded in terms of valence internal coordinates, with parameters calibrated with our own *ab initio* data.[15] The PES was tested by the calculation of rate constants for the elimination reaction [step **c** in Eqn. (3)] and a further comparison between them and the experimental rates. The calculated rate constants were in overall good agreement with experiment when semiclassical corrections to the conventional transition state expression were used.[14] A contour plot of the PES for the methoxy radical in its equilibrium geometry, with nitric oxide in its relaxed geometry moving around, is shown in Fig. 1. The main feature in the plot is the methyl nitrite minimum and the lack of a barrier for the recombination reaction. The minimum energy paths (MEPs; calculated with our PES) involving the elementary steps in Eqn. (3) are displayed graphically in Fig. 2. As seen in Fig. 2, there exists a very tight saddle-point of index one for the elimination reaction with an energy barrier slightly higher than the $CH_3O + NO$ dissociation energy.

In a previous direct dynamics study,[15] we also investigated the elimination and dissociation reactions of methyl nitrite [steps **b** and **c** in Eqn. (3)]. Whereas for the elimination reaction very good agreement with experiment was reached, for the dissociation channel our theoretical rates were substantially higher than those obtained experimentally. The reason for this 'disagreement' was attributed to the underestimation of the CH_3O—NO dissociation energy in the theoretical study,[15] since the dissociation rate constant is very sensitive to the magnitude of this value. In addition, the recombination rate constant is found to be quite sensitive

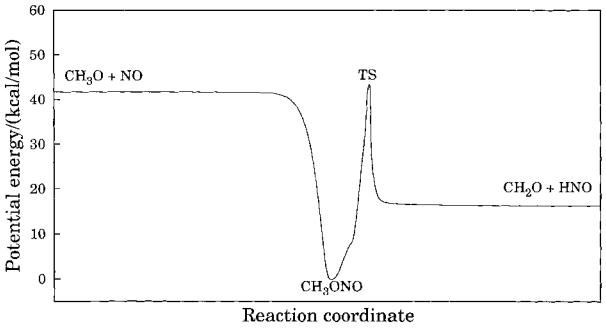

Figure 2. MEPs for the elementary steps in the reaction mechanism in Eqn. (3)

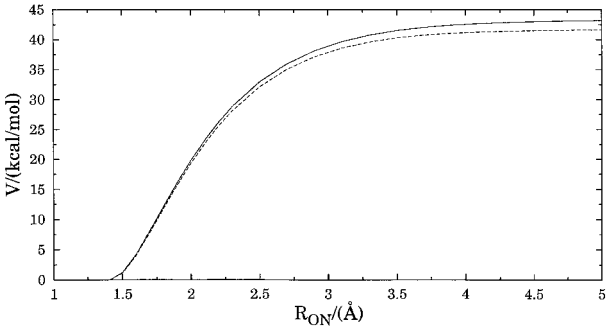

Figure 3. Potential energy profile along the CH_3O—NO distance (methoxy and nitric oxide with relaxed geometries at each step) calculated with the original version of our PES (---) and the modified version of the present work (—)

to the assumed form for the potential.[16] In fact, Hase *et al.*[17] showed that the Morse potential (the one used in our model[14]) is too long range when compared with *ab initio* calculations on the $H + CH_3$ recombination reaction. They proposed a 'stiff' Morse function in which the curvature parameter β varies as a function of the separation of the fragments. However, in the present work, and owing to the lack of accurate long-range *ab initio* calculations, we have made another type of correction to our previously reported surface to obtain a more realistic CH_3O—NO dissociation energy that will produce better results for both the unimolecular dissociation and the recombination rates.[†] More specifically, the new PES includes a switching function of the form:

$$\mathrm{SW} = \{1 - \exp[-a(r_{\mathrm{ON}} - r_{\mathrm{ON}}^{\mathrm{eq}})]\} \times \left\{ \exp\left[- b\left(\sum_i r_{\mathrm{CH(i)}} - r_{\mathrm{CH}}^{\mathrm{eq}} \right) \right] \right\} \quad (4)$$

where $a = 0.5$ Å^{-1} and $b = 10.0$ Å^{-1}; $r_{\mathrm{ON}}^{\mathrm{eq}}$ is the *trans*-methyl nitrite ON equilibrium bond length (see Ref. 14) and $r_{\mathrm{CH}}^{\mathrm{eq}}$ is the methoxy radical CH equilibrium bond length.[14] Thus, SW has a value of one for the $CH_3O + NO$ asymptotic channel and zero for the methyl nitrite equilibrium geometry. This switching function was incorporated into the ON interaction potential (a Morse function; see Ref. 14) in the following way:

$$V(r_{\mathrm{ON}}) = V_{\mathrm{original}}(r_{\mathrm{ON}}) + D \times \mathrm{SW} \quad (5)$$

where $V_{\mathrm{original}}(r_{\mathrm{ON}})$ is the ON interaction term in the original PES, and D is 1.9 kcal mol^{-1}. Our original surface predicted a dissociation energy D_e (zero-point energy excluded) of 41.7 kcal mol^{-1}, whereas the new PES predicts a value of 43.6 kcal mol^{-1} (the corresponding D_0 at 298 K is 41.2 kcal mol^{-1}, which compares quite well with the recommended literature[18] value of 41.8 ± 0.9 kcal mol^{-1}).[‡] Figure 3 shows a cut of both surfaces along the CH_3O—NO distance, with the remaining coordinates relaxed. Because we have used the switching function SW, the new surface only modifies the CH_3O—NO dissociation channel energy; it does not change the remaining attributes of the original PES (i.e. the geometrical and energetic parameters for the elimination channel). Therefore, this surface could be used in a dynamics study to analyze the branching ratios for both channels, which are also of great interest.[1,5,7,11]

CVTST RATE CONSTANTS

According to variational transition state theory, the rate constant can be expressed as[19–23]

$$k(T,s) = \sigma \frac{k_{\mathrm{B}}T}{h} \frac{Q^{\mathrm{ts}}(T,s)}{Q^{\mathrm{R}}(T)} \exp(-V_{\mathrm{MEP}}(s)/k_{\mathrm{B}}T) \quad (6)$$

where σ is the symmetry factor, h and k_{B} are the Planck and Boltzmann constants, $V_{\mathrm{MEP}}(s)$ is the potential energy along the MEP at a given reaction coordinate distance s, and Q^{R} and Q^{ts} are the partition functions of the reactants and the transition state respectively. The conventional transition state rate constant k^{TST} corresponds to $s = 0$ (the saddle point for a reaction with a barrier). In CVTST the transition state is located at the point along the reaction coordinate where the thermal rate constant is minimized.

In terms of the free energy of activation, the thermal rate constant can also be expressed as

$$k(T,s) = \sigma \frac{k_{\mathrm{B}}T}{h} \exp(-\Delta G^{\mathrm{ts}}(T,s)/k_{\mathrm{B}}T) \quad (7)$$

[†]The recombination rates are not as sensitive to the potential well depth as the dissociation rates. However, by making a deeper well depth the potential will be more long range and, consequently, the recombination rates will be higher than those obtained with the previous surface.

[‡]This value is based on Batt's data of Ref. 2.

The agreement could be better by increasing the value 1.9 in Eqn. (5). However, this would affect the dissociation rate constants and also the energetics for the elimination channel. Therefore, the PES could not be used in a more complete kinetic study.

where ΔG^{ts} is the difference in free energy between the transition state and the reactants. The above equation indicates that the minimum in $k(T, s)$ corresponds to a maximum in ΔG^{ts}. Therefore, the best dividing surface (the transition state) is found at the reaction coordinate point at which the free energy change is maximum. Since for the dissociation reaction there is no saddle point, the MEP was calculated starting from an initial CH_3O—NO separation of 10 Å and using a step-size in the numerical integration of 0.001 amu$^{1/2}$ Å.

It is well known that low-frequency vibrations are best treated as two-dimensional hindered internal rotors instead of quantum harmonic normal modes.[24] In fact, we have recently shown that this is also important to predict more realistic kinetic isotope effects and the energy dependence of the microcanonical rate constants.[14] Thus, in the present study the four lowest-frequency vibrations (corresponding to the CH_3O and NO rocking motions) were treated as two hindered two-dimensional rotations. The Hamiltonian for this motion reads

$$H = \frac{p_\theta^2}{2I_\theta} + \frac{p_\varphi^2}{2I_\varphi \sin^2\theta} + V(\theta, \varphi) \tag{8}$$

where θ is bounded by 0 and π and φ by 0 and 2π. The classical partition function for this Hamiltonian is

$$Q = \frac{1}{\sigma h^2} \int \exp(-H/k_B T) \mathrm{d}\Gamma \tag{9}$$

where σ is the symmetry number and the infinitesimal phase space volume $\mathrm{d}\Gamma$ is $\mathrm{d}p_\theta \mathrm{d}p_\varphi \mathrm{d}\theta \mathrm{d}\varphi$.

In the present work, CVTST rate constants were calculated by using Eqn. (7) with the quantum harmonic approximation for all the degrees of freedom at the variational transition state except for the four lowest-frequency vibrations, which were treated as hindered two-dimensional rotors.

The transition state properties for the unimolecular dissociation obtained in this work are collected in Table 1 and compared with the results obtained in our previous direct dynamics study.[15] Equation (7) shows that there are two opposing influences on the magnitude of the free energy variation: the enthalpy change ΔH^{ts} and the entropy change ΔS^{ts}. ΔH^{ts} becomes larger as the separation between the fragments in the transition state increases and the potential $V_{MEP}(s)$ rises to its asymptotic value. Hence the enthalpic effect favors a maximum in ΔG^{ts} at large separations of the fragments (large O—N distances in Table 1). ΔS is also maximized at large separations of the fragments, since the freely rotating products correspond to a maximum in the entropy. Since the ΔS term appears as a negative quantity in the free energy change ($\Delta G^{ts} = \Delta H^{ts} - T\Delta S^{ts}$), this term favors a maximum in ΔG^{ts} at smaller separations in the transition state. In addition, the contribution of the ΔS^{ts} term to the free energy becomes more important as the temperature increases. Therefore, as the temperature increases it is expected to lead to a decrease in the separation between the fragments at the transition state, as shown in Table 1. Also seen in Table 1 is that the direct dynamics calculations of Ref. 15 predict substantially lower separation of the fragments at the transition state than those obtained here with the improved analytical potential, which may be explained by differences in the shapes and reaction endothermicities of the PESs involved.

Table 1. Transition state properties obtained in the CVTST calculations for the dissociation $CH_3ONO \rightarrow CH_3O + NO$

Temperature	R(O—N)^{ts}/Å[a,b]	R(O—N)^{ts}/Å[a,c]	ΔG^{tsd}
300	2.93	3.61	35.54
400	2.93	3.45	34.19
500	2.93	3.31	32.88
600		3.23	31.64
700		3.14	30.47
800		3.09	29.34
1000	2.78	2.66	28.03

[a] CH_3O—NO distance at the variational transition state.
[b] Results from Ref. 15.
[c] CVTST calculations of this work
[d] Free energy variation at the transition state.

The rate constants for the dissociation reaction are collected in Table 2 in comparison with experiment[7] and our previous direct dynamics results.[15] As shown in Table 2, the present dissociation rate constants are in much better agreement than those obtained previously. In particular, this is true at 300 K; whereas the rates obtained in our previous direct dynamics study[15] are about 39 times higher than experiment,[7] the theoretical rates of the present work are only 2.8 times lower. In addition, at 1000 K the rates obtained in the previous direct dynamics study[15] are 2.5 times higher than the experimental ones,[7] whereas the CVTST rates of the present work are only 1.7 times lower. Clearly, a substantial improvement of the theoretical results was achieved in the present work.

The recombination rate constant can also be calculated by CVTST theory from the unimolecular rates by using the following expression:

$$k_{rec}/k_{uni} = K_{eq} \tag{10}$$

where K_{eq} is the equilibrium constant calculated as

$$K_{eq} = \frac{Q_{CH_3ONO}}{Q_{CH_3O} Q_{NO}} \exp(\Delta H_0^\circ / k_B T) \tag{11}$$

where ΔH_0° is the enthalpy difference between the reactant and product at $T = 0$ K and Q_{CH_3ONO}, Q_{CH_3O} and Q_{NO} are the CH_3ONO, CH_3O and NO partition functions.

Table 2. CVTST rate constants (s^{-1}) for $CH_3ONO \rightarrow CH_3O + NO$ and comparison with experiment

Temperature	$k(T)$[a]	$k(T)$[b]	$k_{exp}(T)$[c]
300	8.5 (−12)	7.8 (−14)	2.2 (−13)
400	3.7 (−5)	1.7 (−6)	3.2 (−6)
500	3.8 (−1)	4.3 (−2)	6.5 (−2)
600		3.7 (+1)	4.8 (+1)
700		4.4 (+3)	5.3 (+3)
800		1.6 (+5)	1.8 (+5)
1000	6.6 (+7)	1.5 (+7)	2.6 (+7)

[a] Results from Ref. 15.
[b] CVTST calculations of this work
[c] Experimental results from Ref. 7.

Note that in this case $Q_{CH_3}O$ and Q_{NO} also include the translational and electronic factors. The electronic partition factors, in which spin–orbit coupling was explicitly considered, are[25–30]

$$Q_{CH_3O} = 2 + 2\exp(-141/T) \tag{12}$$

and

$$Q_{NO} = 2 + 2\exp(-177/T) \tag{13}$$

with the temperature in kelvin. The recombination rate constants thus obtained will be presented and compared with experiment and with the results of classical trajectory calculations in the following section. It is interesting to point out that the variable reaction coordinate (VRC) variational transition state theory model of Klippenstein and coworkers[31] may lead to more accurate recombination rates than those obtained here with conventional VTST.

RECOMBINATION RATE CONSTANTS

Although recombination rates can be estimated as shown in the previous section by CVTST calculations, the dynamical details (like, for instance, dividing surface recrossings) are bypassed in the transition state theory approach. Given a PES for a reactive system and not very far from the classical limit, the quasi-classical trajectory calculations are equivalent to a real experiment in the laboratory. Therefore, in the present work we have also performed extensive quasi-classical trajectory calculations for the title recombination reaction.

The quasi-classical trajectory method can be employed to obtain $CH_3O + NO \rightarrow CH_3ONO$ recombination rate constants from the following expression:[32]

$$k(T) = g_e(T)(8kT/\pi\mu)^{1/2}\frac{N_r}{N}\pi b_{max}^2 \tag{14}$$

where μ is the reduced mass of the reactants (CH_3O and NO), N_r the number of reactive events, N the total number of trajectories in the ensemble, b_{max} the maximum impact parameter and $g_e(T)$ the electronic degeneracy factor. The initial conditions were selected as follows: the internal (vibrational and rotational) and relative translational energies of the reactants where chosen from the corresponding Boltzmann distributions.[32] Additionally, the impact parameter was randomly chosen from 0 to b_{max}.

In the present work, quasi-classical trajectory rate constants were calculated using Eqn. (14) for the temperature range 300–1000 K at seven temperatures. Batches of 1000 trajectories were used to determine the maximum impact parameter and ensembles of 10000 trajectories were used to evaluate the reaction probability (N_r/N) for each temperature, so that a total of 154000 trajectories were ran on a UP1000 Alpha platform. To determine whether or not methyl nitrite had been formed, a geometrical test was considered. More specifically, we used a step-size of 0.03 fs until a point in which all the bond distances in CH_3ONO^* dropped below 2 Å or the asymptotic entrance channel was reached again. To evaluate the electronic degeneracy factor $g_e(T)$, spin–orbit splitting of the ^2E states of methoxy[25] and $^2\Pi$ states of nitric oxide[26–30] were explicitly considered, and, therefore, this factor has the following form:

$$g_e(T) = \frac{1}{[2 + 2\exp(-177/T)][2 + 2\exp(-141/T)]} \tag{15}$$

All the trajectory calculations were accomplished by using the VENUS95 dynamics program.[33]

The maximum impact parameters computed in this work for the seven temperatures studied are collected in Table 3. The results presented on the left side of Table 3 were obtained with the original PES.[14] As shown in Table 1, the impact parameter decreases with temperature, since we are studying a reaction without an energy barrier. Also shown is that between 8 and 11% of the trajectories led to CH_3ONO^* for the original PES. In addition, Table 1 collects the corresponding maximum impact parameters and reaction probabilities calculated with the modified version of the surface in the same temperature range. As can be seen, the maximum impact parameter is substantially increased in this new PES, as could be anticipated by a simple inspection of Fig. 3. In addition, the N_r/N ratio was also increased in this case. Though the dissociation rate constants are very much sensitive to the potential well depth, the recombination rate constants are less sensitive to this value. The main influence arises from the change in the position of the variational transition state. That is, with the modified version of the PES we obtain looser variational transition states (i.e. the transition state partition functions values are higher) than those obtained with the previous surface. This is the

Table 3. Impact parameters and reaction probabilities for the title association reaction in the 300–1000 K temperature range

	Original PES[a]		Modified PES[a]	
Temperature	b_{max}	N_r/N_t	b_{max}	N_r/N_t
300	5.5	0.0773	7.4	0.0798
400	5.3	0.0858	6.3	0.1029
500	5.3	0.0868	5.9	0.1125
600	5.1	0.0952	5.8	0.1106
700	5.0	0.1021	5.8	0.1058
800	4.9	0.1072	5.4	0.1216
1000	4.9	0.1082	5.2	0.1251

[a] Values of the maximum impact parameters (Å) and the reaction probabilities N_r/N_t (where N_r is the number of reactive events and N_t the total number of trajectories).

main reason why the modified version gives higher recombination rate constants.

The rate constants calculated with our original PES by classical trajectory calculations are shown in Fig. 4 (open circles connected by a line for visual clarity) along with the experimental results of Caralp *et al.*[13] (solid line), Frost and Smith[8] (dashed line), Sanders *et al.*[3] (full triangles), Zellner[4] (full squares) and Ohmori *et al.*[10] (full circles). The classical trajectory rate constants computed with our modified surface are shown as dot circles. Also, the CVTST rate constants of the present work are depicted in Fig. 4 as squares. As seen in Figure 4, the CVTST rates are upper bounds to the 'exact' classical rate constants (those obtained by quasi-classical trajectory calculations). In addition, the CVTST recombination rates predict a marked temperature dependence, not observed in the classical trajectory nor in the experiment. The maximum difference between the CVTST and the trajectory recombination rate constants appears at the highest temperatures (at 800 K the CVTST rate is almost five times greater than the trajectory one). This difference may be explained on the basis of the dynamical effects 'bypassed' in the statistical CVTST calculations. For example, the recrossings of the dividing surface, which are more often at high temperatures, are only taken into account in the statistical model by minimizing the rate constant with respect to the dividing surface location, whereas in the classical trajectory model the trajectories are followed up to the CH_3ONO well; i.e. the transition state recrossings are properly taken into account. Overall, owing to the approximations employed to evaluate the CVTST recombination rate constants (see section above), the results are quite reasonable. As seen in Fig. 4, most of the experimental rates are reported for room temperature and present a wide scattering. Therefore, the comparison between theory and experiment is reasonably good, especially for the theoretical results obtained with the modified PES. The quasi-classical trajectory results obtained with our new surface do not exhibit temperature dependence, whereas those obtained with the original one present a temperature dependence contrary to that suggested by Caralp *et al.*[13] and Frost and Smith.[8] However, we must stress at this point that the experimental values were not measured directly but derived by fitting the experimental rates to RRKM and/or Lindemann–Hinshelwood equations. Also seen in Fig. 4 is that the differences between the quasi-classical rate constants

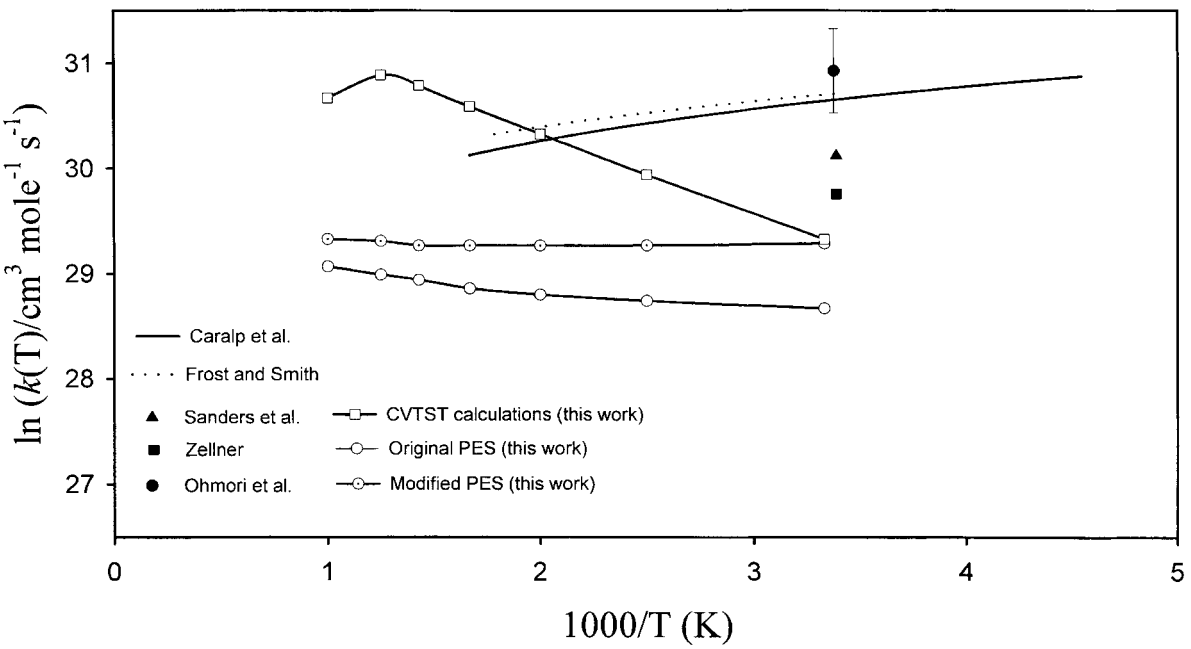

Figure 4. Comparison between the thermal rate constants computed in this work and those obtained experimentally. See the legends of the figure

calculated by the two PESs increase as the temperature decreases. Therefore, the lower-temperature calculations are more sensitive to the shape of our PES. To some extent, the discrepancies between our calculated and the experimental rates could be attributed to the lack of an accurate treatment of the long-range interactions, which influence the precise value for the recombination rates[34,35] as stated above. Overall, taking into account the agreement between the experimental results of He *et al.*[7] and our CVTST dissociation rate constants and the scattering in the experimental recombination rate constants (Fig. 4), our model PES seems to be quite satisfactory.

CONCLUSIONS

In the present study, classical trajectory and CVTST calculations were performed to calculate thermal rate constants for the experimentally well-studied methoxy + nitric oxide reaction. In particular, we focused on the recombination rates to give chemically activated methyl nitrite, which can subsequently undertake a four-center elimination reaction (studied previously[14,15]) or can dissociate to give methoxy and nitric oxide again. The classical rates computed in the present work compare reasonably well with the experimental rates at the lowest temperature (300 K) taking into account the scattering in the experimental results. We improved our results by modifying our original PES to obtain a more reliable dissociation energy for the CH_3O—NO bond. The rate constants obtained with this new surface compare better with experiment, but they still differ to some extent. Overall, taking into account the agreement between the theoretical rates obtained with our new model and those determined experimentally, the new PES seems to be substantially improved after the modification made in the present work.

Acknowledgements

E.M.-N. and S.A.V. are pleased to acknowledge the financial support from Ministerio de Ciencia y Tecnología, Spain (BQU2000-0462). We would also like to acknowledge helpful discussions with Dr J. M. C. Marques from Universidade de Coimbra (Portugal).

REFERENCES

1. Glasson WA. *Environ. Sci. Dep. Technol.* 1975; **9**: 1048.
2. Batt L, Milne RT, McCulloch RD. *Int. J. Chem. Kinet.* 1977; **9**: 567.
3. Sanders N, Butler JE, Pasternack LR, McDonald JR. *Chem. Phys.* 1980; **49**: 17.
4. Zellner R. *J. Chim. Phys.* 1987; **84**: 403.
5. Jenkin ME, Hayman GD, Cox RA. *J. Photochem. Photobiol. A* 1988; **42**: 187.
6. Zaslonko IS, Mukoseev YK, Tyurin AN. *Kinet. Katal.* 1988; **29**: 283.
7. He Y, Sanders WA, Lin MC. *J. Phys. Chem.* 1988; **92**: 5474.
8. Frost MJ, Smith IWM. *J. Chem. Soc. Faraday Trans.* 1990; **86**: 1757.
9. McCaulley JA, Moyle AM, Golde MF, Anderson SM, Kaufman F. *J. Chem. Soc. Faraday Trans.* 1990; **86**: 4001.
10. Ohmori K, Yamasaki K, Matsui H. *Bull. Chem. Soc. Jpn.* 1993; **66**: 51.
11. Dobe S, Lendvay G, Szilagyi I, Berces T. *Int. J. Chem. Kinet.* 1994; **26**: 887.
12. Daele V, Laverdet G, Le Bras G, Poulet G. *J. Phys. Chem.* 1995; **99**: 1470.
13. Caralp F, Rayez MT, Frost W, Gomez N, Delcroix B, Fittschen C, Devolder P. *J. Chem. Soc. Faraday Trans.* 1998; **94**: 3321.
14. (a) Martínez-Núñez E, Vázquez SA. *J. Chem. Phys.* 1998; **109**: 8907; (b) Martínez-Núñez E, Vázquez SA. *J. Chem. Phys.* 1999; **111**: 10–501.
15. Fernández-Ramos A, Martínez-Núnez E, Ríos MA, Rodríguez-Otero J, Vázquez SA, Estévez CM. *J. Am. Chem. Soc.* 1998; **120**: 7594.
16. Hase WL, Duchovic RJ. *J. Chem. Phys.* 1985; **83**: 3448.
17. Hase WL, Mondro SL, Duchovic RJ, Hirst DM. *J. Am. Chem. Soc.* 1987; **109**: 2916.
18. Weast RC (ed.). *Handbook of Chemistry and Physics*, vol. 67. CRC Press: Boca Raton, FL, 1986–87.
19. Hase WL, Duchovic RJ. *J. Chem. Phys.* 1985; **76**: 1380.
20. Quack M, Troe J. *Ber. Bunsenges. Phys. Chem.* 1977; **81**: 329.
21. Truhlar DG, Garret BC. *Acc. Chem. Res.* 1980; **13**: 440.
22. Truhlar DG, Hase WL, Hynes JT. *J. Phys. Chem.* 1983; **87**: 2644.
23. Truhlar DG, Isaacson AD, Garret BC. In *Theory of Chemical Reaction Dynamics*, Baer M (ed.). Chemical Rubber Company: Boca Raton, FL, 1985.
24. Gilbert RG, Smith SC. In *Theory of Unimolecular and Recombination Reactions*. Blackwell: Oxford, 1990; 95.
25. Brossard SD, Carrick PG, Chappell EL, Hulegaard SC, Engelking PC. *J. Chem. Phys.* 1986; **84**: 2459.
26. Engelman Jr R, Rouse PE, Peek PE, Baiamonte PE. Beta and gamma band systems of nitric oxide, Rpt. LA-4364 1970; vol. **1**.
27. Valentin A, Boissy JP, Cardinet P, Henry A, Chen DW, Rao KN. *Acad. Sci. Paris Ser. B* 1976; **283**: 233.
28. Johns JWC, Reid J, Lepard DW. *J. Mol. Spectrosc.* 1977; **65**: 155.
29. Brown JM, Cole ARH, Honey FR. *Mol. Phys.* 1972; **23**: 287.
30. Mizushima M, Evenson KM, Wells JS. *Phys. Rev. A* 1972; **5**: 2276.
31. (a) Sawilowsky EF, Klippenstein SJ. *J. Phys. Chem. A* 1998; **102**: 9811; (b) Klippenstein SJ, Allen WD. *Ver. Bunsen. Ges.* 1997; **101**: 423; (c) Klippenstein SJ, Yang Y-C, Ryzhov V, Dunbar RC. *J. Chem. Phys.* 1996; **104**: 4502.
32. Peslherbe GH, Wang H, Hase WL. *Adv. Chem. Phys.* 1999; **105**: 171.
33. Hase WL, Duchovic RJ, Hu X, Lim KF, Lu DH, Peslherbe GH, Swamy KN, Vande Linde SR, Wang H, Wolf RJ. VENUS 95, a General Chemical Dynamics Computer Program. VENUS 95 is an enhanced version of MERCURY: Hase WL. QCPE#453.
34. Clary DC, Henshaw JP. *Faraday Discuss. Chem. Soc.* 1987; **84**: 333.
35. Varandas AJC. *Faraday Discuss. Chem. Soc.* 1987; **84**: 353.